ChemPubSoc Europe

DOI: 10.1002/ejic.201600121

EurJIC European Journal of Inorganic Chemistry

Full Paper

Hydrogen Activation

Computational Insights into the Mechanisms of H_2 Activation and H_2/D_2 Isotope Exchange by Dimolybdenum Tetrasulfide Complexes

Andrés G. Algarra*[a]

Abstract: The mechanisms for H_2 activation by $[Cp^*Mo]_2(\mu\text{-}S)_2(\mu\text{-}S_2)$ (**1-a**, Cp^* = pentamethylcyclopentadienyl) and its reaction product $[Cp^*Mo]_2(\mu\text{-}S)_2(\mu\text{-}SH)_2$ (**2**) have been investigated by DFT methods. The reaction of **1-a** involves the homolytic addition of H_2 to its μ-S ligands, followed by the cleavage of the S–S bond of the $\mu\text{-}S_2$ ligand in a subsequent step. Complex **2** can adopt five conformations that only differ in the stereochemistry of the μ-SH and μ-S ligands; although an isomer with adjacent μ-S ligands (**2-a**) is formed initially, it then isomerises into the experimentally observed **2-d**. This species promotes H/D scrambling in H_2/D_2 mixtures, and the mechanism of the process has also been studied. Notably, all of the computed pathways for the addition of D_2 to **2-d** present prohibitive barriers; instead, only those isomers with adjacent μ-S ligands are able to react further. The homolytic activation of D_2 by these leads to isomers of $[Cp_2Mo_2(\mu\text{-}SH)_2(\mu\text{-}SD)_2]$, the interconversion of which is the rate-determining step.

Introduction

Group 6 transition-metal sulfide complexes are involved in several highly important chemical processes. In the solid state, molybdenum sulfides have been used and studied as catalysts for the hydrodesulfurisation (HDS) of fossil fuels under H_2 pressure,[1] an operation that involves the cleavage of C–S bonds to generate H_2S and sulfur-free hydrocarbons. More recently, MoS_2 nanoparticles have also shown great promise as low-cost alternatives to Pt for the hydrogen evolution reaction (HER).[2] In solution, metal sulfide complexes also have remarkable activities; for example, they appear in the active centres of many metalloenzymes[3] such as nitrogenases, which produce NH_3 from N_2 and H_2, or hydrogenases, which reversibly catalyse the conversion of H_2 into protons and electrons.[4] In addition, some of these species present reactivity patterns similar to those of their heterogeneous counterparts and have therefore been employed as models for such processes.[5]

In a broad sense, two possible pathways have been identified for the activation of H_2 by transition-metal complexes, namely, homolytic and heterolytic activation.[6] In general, electron-rich metal complexes favour homolytic activation (Scheme 1, a) through an oxidative addition mechanism, whereas heterolytic activation (Scheme 1, b) often occurs in the presence of electron-poor metals and formally leads to H^- and H^+ ions. For chalcogenide-containing complexes, there are examples of species in which sulfur and oxygen donor ligands behave as proton acceptors through mechanisms that imply the [2+2] addition of H_2 across the M–Q (Q = chalcogenide) bond (also known as σ-bond metathesis,[7] Scheme 1, c),[8–10] as well as cases in which H_2 is activated without the direct participation of the metal atom through the [3+2] addition to a *cis*-MQ_2 moiety of the complex (Scheme 1, d).[11]

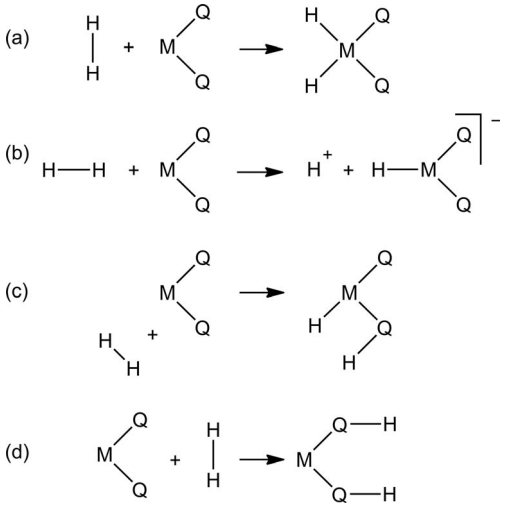

Scheme 1.

Dimolybdenum tetrasulfide complexes feature the same Mo/S ratio as nanoparticulate MoS_2 and have been studied extensively because of their ability to activate H_2 and undergo C–S bond-formation reactions with alkenes and alkynes.[9,12–16] Specifically, $[Cp^*_2Mo_2S_4]$ (**1**, Cp^* = pentamethylcyclopentadienyl)

[a] *Departamento de Ciencia de los Materiales e Ingeniería Metalúrgica y Química Inorgánica, Universidad de Cádiz, Campus Universitario de Puerto Real, 11510 Puerto Real, Cádiz, Spain*
E-mail: andres.algarra@uca.es

Supporting information and ORCID(s) from the author(s) for this article are available on the WWW under http://dx.doi.org/10.1002/ejic.201600121.

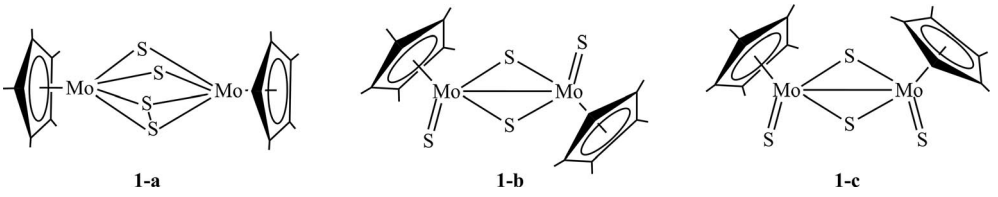

Scheme 2. Experimentally characterised structures of $Cp^*_2Mo_2S_4$: $[Cp^*Mo]_2(\mu\text{-}S)_2(\mu\text{-}S_2)$ (**1-a**),[19] *anti*-$[Cp^*MoS]_2(\mu\text{-}S)_2$ (**1-b**)[13j] and *syn*-$[Cp^*MoS]_2(\mu\text{-}S_2)$ (**1-c**).[25]

can exist as three different isomeric structures (see Scheme 2), and experimental[17] and computational[18] studies have shown that the interconversions between them can be thermally[19] or photochemically[17] promoted. Fortunately, although **1-b** is the most stable isomer,[20] the synthetic method of Wachter et al. under mild reaction conditions allows the isolation of **1-a**,[19,21] the reactivity of which has proven especially remarkable. Indeed, if H_2 (1 atm) is added to a CH_2Cl_2 solution of **1-a**, the formation of $[Cp^*Mo]_2(\mu\text{-}S)_2(\mu\text{-}SH)_2$ (**2**) is quantitative within 90 min in a process that involves the cleavage of the S–S bond of the $\mu\text{-}S_2$ moiety in **1-a**.[14] The existence of such a bond, which also explains why an isomeric structure of formula $[Cp^*Mo]_2(\mu\text{-}S)_4$ has not been observed, has been justified as a consequence of the relief of the lone-pair–lone-pair repulsion between the bridging sulfur ligands.[18b] Clearly, owing to the formation of two S–H bonds in **2**, this is no longer necessary, and the S–S bond is broken. From a computational point of view, Fenske–Hall molecular orbital calculations have shown that the lowest unoccupied molecular orbital (LUMO) of **1-a** features significant sulfur character and the correct symmetry to act as an acceptor of the π bonds of olefins or the σ bond of H_2.[15,18]

The structure and reactivity of $Cp^*_2Mo_2S_4H_2$ (**2**) has also received great attention, and it can adopt five isomeric structures that only differ in the stereochemistry of the hydrosulfido groups (see Scheme 3).[16] Although the initial isomer resulting from the reaction with H_2 is likely to be **2-a**, the isomer observed experimentally is **2-d**, as first assigned by Rakowski DuBois et al. on the basis of ^1H NMR spectroscopic data[15] and later predicted by Franz et al.[22] on the basis of DFT calculations.[23] Interestingly, although the product resulting from the addition of a second H_2 molecule to **2-d** is not a stable species, this dinuclear compound does catalyse the formation of HD in the presence of a mixture of H_2/D_2.[13k] Specifically, Rakowski DuBois et al. reported that if H_2 (0.75 atm) and D_2 (0.25 atm) are added to a degassed solution of **2-d** in benzene, approximately 12 % of HD is observed after the mixture has been stirred at 25 °C for 3 d.

In spite of the wide range of investigations on the structure and properties of these dimolybdenum tetrasulfide complexes and some of their structural analogues,[16,22,24] to the best of our knowledge, no DFT study has been performed to determine the mechanistic details of H_2 activation by **1-a** or the role of **2-d** in the H/D scrambling in H_2/D_2 mixtures. Thus, in this manuscript, a computational study aimed to provide insights into the fundamental aspects of the structures and reactivity of these species with H_2 is presented. The results are organised as follows: first, a mechanistic study on the reaction between **1-a** and H_2 is presented; next, the interconversion between the isomers of the resulting product $[Cp^*Mo]_2(\mu\text{-}S)_2(\mu\text{-}SH)_2$ is analysed; and, lastly, their role in the formation of HD in H_2/D_2 mixtures is shown.

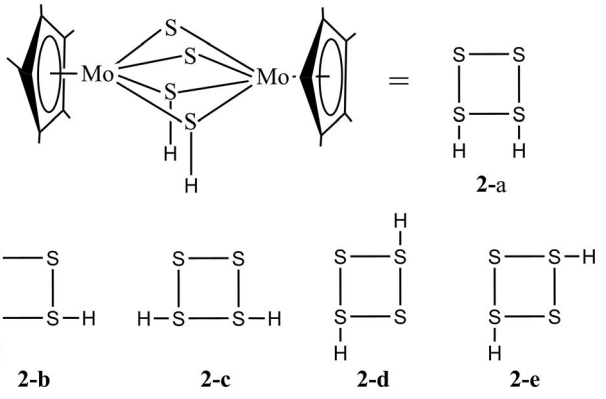

Scheme 3. Structural representations of the isomeric structures of $[Cp^*Mo]_2(\mu\text{-}S)_2(\mu\text{-}SH)_2$ viewed down the Mo–Mo axis.[26]

Results and Discussion

The Structure of $[Cp^*Mo]_2(\mu\text{-}S)_2(\mu\text{-}S_2)$ and Its Reaction with H_2

The computational study was started with the optimisation of the structure of **1-a** and the comparison of the results with its X-ray[19] structure (see Figure 1). The analysis of the main geometrical parameters for both geometries shows that they are in good agreement, although a small overestimation of the metal–metal and metal–sulfur bond lengths, typically associated with the use of the B3LYP functional,[27] is observed (see Figure 1 and Table S1). Nonetheless, the calculations reproduce

	1-a	1-d	1-e
Mo^1-Mo^2	2.62 (2.60)	2.75	2.61
Mo^1-S^1	2.38 (2.36)	2.49	2.32
Mo^1-S^3	2.52 (2.45)	2.49	2.53
S^1-S^2	3.15 (3.10)	2.11	2.90
S^3-S^4	2.12 (2.10)	2.11	2.91

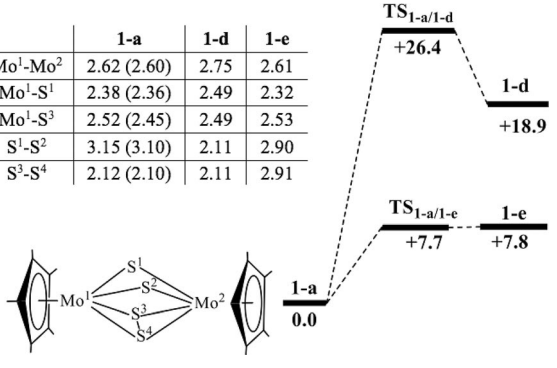

Figure 1. Computed free-energy profile [kcal mol^{-1}] for the isomerisation of **1-a** into **1-d** and **1-e**. The distances in the table are given in Å, and the experimental X-ray values for **1-a** are included in parentheses.

the μ-S_2 and (μ-S)$_2$ groups of the X-ray structure, which present markedly different sulfur–sulfur distances. It is possible to computationally optimise geometries resulting from the formation of a S–S bond between the two μ-S groups in **1-a**, that is, [Cp*$_2$Mo$_2$(μ-S_2)$_2$] (**1-d**), and from the cleavage of the S–S bond in **1-a**, that is, [Cp*$_2$Mo$_2$(μ-S)$_4$] (**1-e**). The free-energy profiles for such transformations are also included in Figure 1, and it can be seen that **1-d** and **1-e** are less stable than **1-a** by 18.9 and 7.8 kcal mol^{-1}, respectively, and their formations present free-energy barriers of 26.4 (TS**1-a/1d**) and 7.7 kcal mol^{-1} (TS**1-a/1e**, see structures in Figure S1). These results are in line with extended Hückel calculations by Hoffmann et al. on the cyclopentadienyl analogues of **1-a**, **1-d** and **1-e**[18c] and generally agree with the experimental observation of **1-a**.

Several pathways for the activation of H_2 in the presence of **1-a** have been analysed computationally (Scheme 4). Given that both hydrogen atoms of H_2 form part of the final species, the possible heterolytic mechanisms are reduced to the addition of H_2 across a Mo(μ-S) moiety of **1-a**, and this is labelled as pathway A. Note that an analogous mechanism could be envisaged across a Mo centre and one of the sulfur atoms of the (μ-S)$_2$ ligand; however, calculations on the hypothetical product showed it not to be a stable species on the potential energy surface (PES). Homolytic mechanisms can proceed through the interaction of H_2 either with one of the molybdenum centres of **1-a** (Pathway B) or with its bridging sulfur ligands. In relation to the latter possibility, and owing to the geometry of **1-a**, dihydrogen can approach the cluster at three inequivalent sides of the square formed by its four sulfur atoms, that is, the dihydrogen molecule can interact with the μ-S_2 ligand (Pathway C), with one μ-S ligand and one of the sulfur atoms of the μ-S_2 ligand (Pathway D), or with the two μ-S ligands (Pathway E).

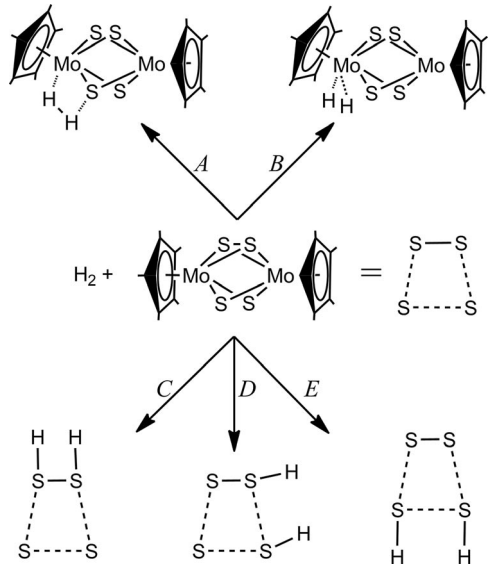

Scheme 4. Mechanistic pathways computed for the addition of H_2 to **1-a**. For simplicity, in some cases, **1-a** has only been represented as the square formed by its four sulfur atoms, and the two sulfur atoms at the top represent the μ-S_2 ligand.

H_2 activation by Pathway A is computed to have an activation free-energy barrier of 52.5 kcal mol^{-1} (TS**1-a/3**). In addition, the formation of **3** is endergonic by 21.1 kcal mol^{-1} (see structures in Figure 2); therefore, such a mechanism can be ruled out. This result is in line with the computed barrier of 43 kcal mol^{-1} for the same process with Cp$_2$Mo$_2$(μ-SH)(μ-S)(μ-S_2CH$_2$), which was explained on the basis of the disruption of the Mo–S π bonding in the reactant.[10] In the present case, the activation strain model (ASM) analysis of TS**1-a/3** clearly agrees with such a description, as it shows that almost 90 % of the activation barrier comes from the deformation of the dinuclear cluster (see Table 1). The oxidative addition of H_2 to one of the molybdenum centres (Pathway B) can also be discarded, as calculations show that both dihydrogen and dihydride reaction products do not represent stationary points on the PES. Similarly, the computation of the structure resulting from the addition of H_2 to the μ-S_2 ligand of **1-a** by Pathway C inevitably leads to the cleavage of the S–S bond and, thus, allows us to rule out this mechanism.

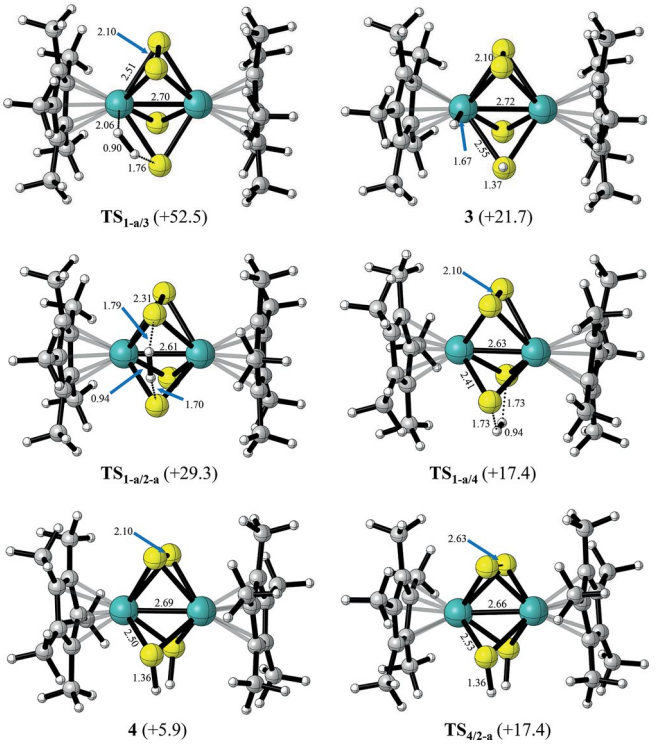

Figure 2. DFT-optimised structures for Pathways A, D and E in Scheme 4. The distances are in Å, and the numbers in parentheses correspond to the free energies [kcal mol^{-1}] relative to the separated reactants (i.e., **1-a** and H_2).

Table 1. Activation strain model (ASM) analysis of the rate-determining transition states for Pathways A, B and C in Scheme 4. The energies [kcal mol^{-1}] are relative to **1-a** + H_2.

	$\Delta G^{\#}$	$\Delta E^{\#}$	$\Delta E^{\#}_{strain}$(**1-a**)	$\Delta E^{\#}_{strain}$(H_2)	$\Delta E^{\#}_{int}$
TS**1-a/3**	52.5	48.2	41.9	7.9	–1.6
TS**1-a/2-a**	29.3	24.5	7.1	10.8	6.6
TS**1-a/4**	17.4	11.8	3.5	10.7	–2.4

The activation of H_2 by Pathway D leads directly to **2-a** in a process that involves the concerted formation of two S–H σ bonds and the cleavage of the S–S bond of the μ-S_2 ligand of **1-a** and the H–H bond of H_2. As expected, the associated transi-

tion state TS**1-a/2-a** features a slightly elongated μ-S_2 sulfur–sulfur bond length (2.309 Å, cf. 2.12 Å in **1-a**), and the same effect is observed in the H–H bond length of H_2 (0.94 Å, cf. 0.74 Å in H_2). Energetically, the process presents a computed free-energy barrier of 29.3 kcal mol^{-1}, and the formation of **2-a** is exergonic by 3.1 kcal mol^{-1} (see Figure 3). In contrast, Pathway E consists of a stepwise mechanism in which the cleavage of the S–S bond of the μ-S_2 ligand and the H–H σ bond of H_2 occur in different steps.

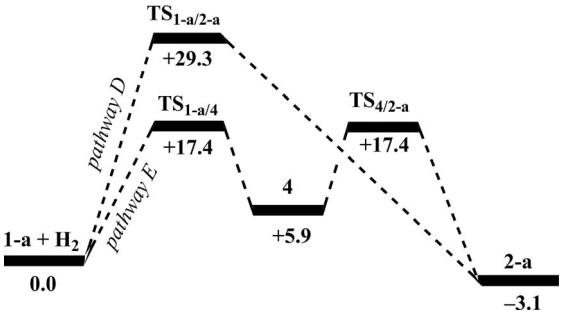

Figure 3. Computed free-energy profiles [kcal mol^{-1}] associated with Pathways D and E in Scheme 4.

Thus, the initial approach of H_2 parallel to the two sulfido groups of **1-a** generates intermediate **4**, which features two S–H bonds (d_{S-H} = 1.37 Å), and the μ-S_2 ligand of the cluster remains intact, that is, a similar sulfur–sulfur bond length of 2.10 Å is computed for the μ-S_2 ligand in **1-a**, TS**1-a/4** and **4** (see Figure 2). The cleavage of the sulfur–sulfur bond occurs in a subsequent step via TS**4/2-a**, which presents a S–S distance of 2.63 Å that is intermediate between those of **4** (2.10 Å) and the reaction product **2-a** (3.11 Å). Interestingly, the free-energy profile for the formation of **2-a** by Pathway E, included in Figure 3, shows that both TS**1-a/4** and TS**4/2-a** feature the same relative free energy of 17.4 kcal mol^{-1}; therefore, it is difficult to determine computationally which of them is rate-determining. Nonetheless, these results clearly point towards Pathway E as the most plausible reaction mechanism for the formation of **2-a**.

At this point, it is interesting to compare the transition states for the H_2 activation by Pathways D (TS**1-a/2-a**) and E (TS**1-a/4**) using the activation strain model. The values in Table 1 show that the cost to deform H_2, $\Delta E^{\#}_{strain}(H_2)$, is very similar in both cases, and the differences appear mainly in terms of $\Delta E^{\#}_{strain}$(**1-a**) and the interaction energy $\Delta E^{\#}_{int}$ between the deformed reactants. The slightly larger $\Delta E^{\#}_{strain}$(**1-a**) associated with Pathway D can be explained by considering that it involves the cleavage of the S–S bond of the μ-S_2 moiety, whereas this happens in a subsequent step in Pathway E. However, the crucial difference between the two TS geometries appears in the $\Delta E^{\#}_{int}$ values, which show a stabilising interaction of 2.5 kcal mol^{-1} for TS**1-a/4**, whereas for TS**1-a/2-a** it is destabilising by 6.6 kcal mol^{-1}.[28] This can be ascribed to the degree of orbital interaction between the reactants at both transition states, and its origin can be traced by analysing the frontier molecular orbitals of the cluster and H_2 in such structures. In agreement with the similar $\Delta E^{\#}_{strain}(H_2)$ and H–H bond length of H_2 in TS**1-a/4** and TS**1-a/2-a**, negligible differences are found in the compositions of the highest occupied molecular orbital (HOMO, σ) and LUMO (σ*) of this fragment at both geometries. The HOMOs of the cluster fragment at both TS geometries also show similar features and are mainly centred at the d orbitals of the molybdenum atoms. This prevents any orbital interaction with the LUMO of H_2; therefore, in both cases, the only mechanism of orbital stabilisation necessarily involves the other possible HOMO–LUMO pair, that is, the HOMO of H_2 and the LUMO of **1-a**. Indeed, clear differences are observed in the composition of the latter. The LUMO of the cluster in TS**1-a/4** is delocalised over the molybdenum centres and the μ-S groups, the contribution of which has the correct symmetry to interact with the σ bond of H_2 (see qualitative representation in Scheme 5). This clearly explains the high degree of orbital interaction and is also consistent with previous theoretical calculations[15,18] Conversely, although the LUMO of **1-a** at the TS**1-a/2-a** geometry is also delocalised over the two molybdenum centres, the contribution of the sulfur atoms is very different in this case. As depicted in Scheme 5, now only one sulfur atom is able to interact with the approaching H_2 molecule, but such an interaction is antibonding owing to the opposite wave-function phases of the two fragments.

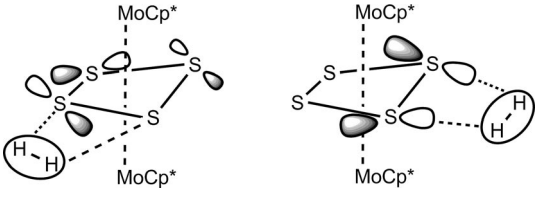

Scheme 5. Orbital interaction between the HOMO of H_2 and the LUMO of **1-a** at the TS**1-a/2-a** (left) and TS**1-a/4** (right) geometries. For simplicity, the orbital contributions of the MoCp* groups have not been drawn (see Figure S2).

The Isomeric Forms of [Cp*Mo]$_2$(μ-S)$_2$(μ-SH)$_2$

As shown in Scheme 3, [Cp*Mo]$_2$(μ-S)$_2$(μ-SH)$_2$ can adopt five different conformations that only differ on the stereochemistry of the sulfido and hydrosulfido ligands. Their structures, as well as those of the transition states for their interconversions, have been computed, and the results are summarised in Figure 4. In agreement with previous DFT calculations on the relative stability of these isomers,[22] **2-d** is computed to be the global minimum, although the other conformer featuring opposite hydrosulfido groups, **2-e**, is only 1.6 kcal mol^{-1} less stable. Conversely, the isomers with adjacent μ-SH groups, that is, **2-a**, **2-b** and **2-c**, are ca. 8–13 kcal mol^{-1} less stable. On the basis of the structural features and relative free energies, the transition states for the interconversion between these conformers can be classified in two groups, those in which the H atoms of the hydrosulfido ligands remain bound to the same sulfur atom (TS**2-a/2-b**, +17.5 kcal mol^{-1}; TS**2-b/2-c**, +21.2 kcal mol^{-1}; TS**2-d/2-e**, +14.8 kcal mol^{-1}) and those that involve hydrogen migration to the adjacent sulfido ligand (TS**2-b/2-e**, +6.6 kcal mol^{-1}; TS**2-c/2-d**, +10.9 kcal mol^{-1}). The former group implies the opening of the cluster core to allow for the change in the orientation of the hydrogen atom within the same hydrosulfido ligand; there-

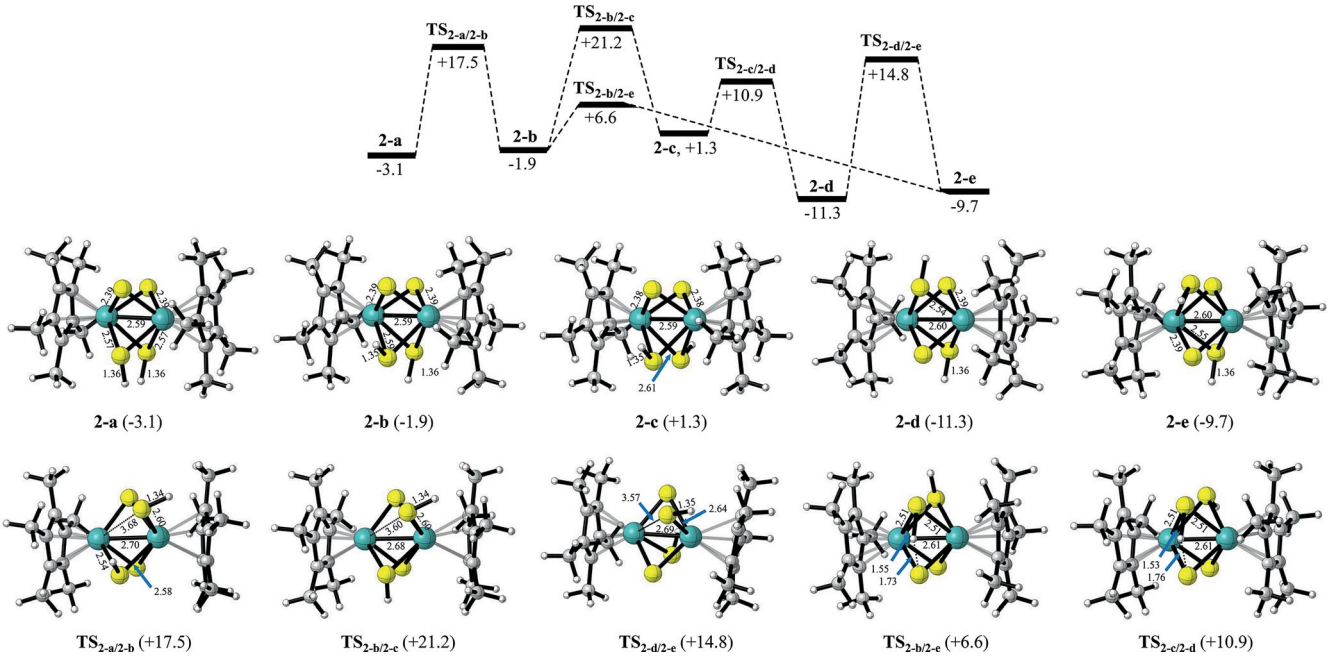

Figure 4. Computed free-energy profile for the interconversion between the isomers of **2**. The numbers in parentheses correspond to the free energies [kcal mol^{-1}] relative to **1-a** + H_2, and selected distances are given in Å.

fore, these TSs do not lead to changes in the overall adjacent or opposite configuration of the sulfido and hydrosulfido ligands. As indicated above, these TSs feature larger activation barriers than the second group (TS**2-b/2-e** and TS**2-c/2-d**), in which the hydrogen atom migrates to an adjacent sulfido ligand in a process that occurs without large cluster distortions. Notably, these TSs resemble, both structurally and energetically, those obtained by McGrady et al. during a mechanistic study of the cleavage of H_2 by $[CpMo]_2(\mu\text{-}SH)(\mu\text{-}S)(\mu\text{-}S_2CH_2)$, for which the low energy barrier for hydrogen migration was explained as formally resulting from the movement of a proton over a continuous cloud of nonbonding electron density located at the metal-based d orbitals and sulfur-based lone pairs.[10] Overall, according to the free-energy profile in Figure 4, it is expected that the formation of **2-a** from the reaction between **1-a** and H_2 will lead to a Boltzmann distribution of isomers, and **2-d** will be the predominant species in solution. These five isomeric structures can be reached through the series of isomerisations **2-a** → **2-b** → **2-e** → **2-d** → **2-c**, for which the rate-determining transition state (TS**2-a/2-b**, +17.5 kcal mol^{-1}) features a computed relative free energy analogous to that associated with the formation of **2-a** from **1-a** and H_2.

In relation to the field of heterogeneous catalysis,[29] it is worth noting that the present results for the addition of H_2 to **1-a** and the subsequent isomerisations of **2-a** bear similarities to the H_2 activation at the edge sites of the MoS_2 crystals employed for hydrodesulfurisation (HDS).[30,31] Particularly, computational studies on the homolytic addition of H_2 to the S–S groups at the 100 % sulfur-covered (10–10) Mo edges of MoS_2 have shown that the formation of a structure analogous to **2-a** is roughly thermoneutral.[31] This has been ascribed to steric constraints between the two protons, which were computed to be separated by only 1.77 Å (cf. 1.95 Å in **2-a**). Nonetheless, such a solid-state structure was not found to be the most stable one, and the rotation of the hydrogen atoms to produce a conformation in which they are placed further away made the process clearly exothermic.

The Reaction of $[Cp^*Mo]_2(\mu\text{-}S)_2(\mu\text{-}SH)_2$ with H_2/D_2 Mixtures and the Formation of HD

As stated above, although $[Cp^*Mo]_2(\mu\text{-}S)_2(\mu\text{-}SH)_2$ does not lead to any other stable adduct in the presence of H_2 (or D_2), it catalyses the formation of HD if H_2 and D_2 are bubbled into a solution of the dinuclear complex.[13k] Although the process was described more than 30 years ago, its mechanistic understanding is still lacking. Using H_2 as a model for D_2, the results of a DFT study to gain insights into the mechanism are presented in this section.

Notably, $[Cp^*Mo]_2(\mu\text{-}S)_2(\mu\text{-}SH)_2$ reacts with alkynes to form species that feature two dithiolate ligands in a process that implies the elimination of H_2 (Scheme 6).[13k] In analogy with this reactivity and with consideration of the results in the previous sections, the formation of species with four hydrosulfido ligands $[Cp_2Mo_2(\mu\text{-}SH)_4]$ can be hypothesised to occur through the activation of H_2 by **2-a**, **2-b** and **2-c**, that is, the isomers of $[Cp^*Mo]_2(\mu\text{-}S)_2(\mu\text{-}SH)_2$ with adjacent sulfido ligands. The structures of the resulting isomers of $[Cp_2Mo_2(\mu\text{-}SH)_4]$, namely, **5-a**, **5-b** and **5-c**, are shown in Figure 5. Again, it is worth noting that these isomers, as well as the transition states for their formation, only differ in the stereochemistry of the hydrosulfido ligands. Although the activation barriers for the formation of these species, of ca. 22–26 kcal mol^{-1}, are typical of reactions that occur at room temperature, the calculations show that the formation of these species is endergonic by ca. 5–6 kcal mol^{-1}

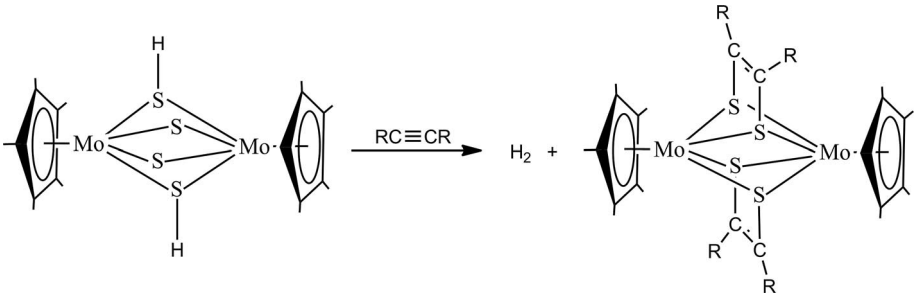

Scheme 6. General reaction of $[Cp^*Mo]_2(\mu\text{-}S)_2(\mu\text{-}SH)_2$ with alkynes.[13k]

(note that isomer **2-d** plus H_2 has to be taken as zero in relative free energy), in agreement with the absence of the experimental evidence of species with molecular formula $[Cp_2Mo_2(\mu\text{-}SH)_4]$. Structurally, these three TSs resemble TS**1-a/4**. Their similarities, both in terms of structure and relative energy, indicate that the stereochemistry of the spectator hydrosulfido ligands does not affect the H_2 addition significantly, and similar conclusions can be applied to the resulting isomers of $[Cp_2Mo_2(\mu\text{-}SH)_4]$. On the other hand, given the arrangement of sulfido and hydrosulfido ligands in **2-d** and **2-e**, a similar process from these species would lead to highly unstable compounds of formula $[Cp_2Mo_2(\mu\text{-}SH)_2(\mu\text{-}SH_2)(\mu\text{-}S)]$, and the computations show that such processes feature activation barriers of ca. 60 kcal mol^{-1} and reaction free energies larger than 40 kcal mol^{-1} (see Figure S3).

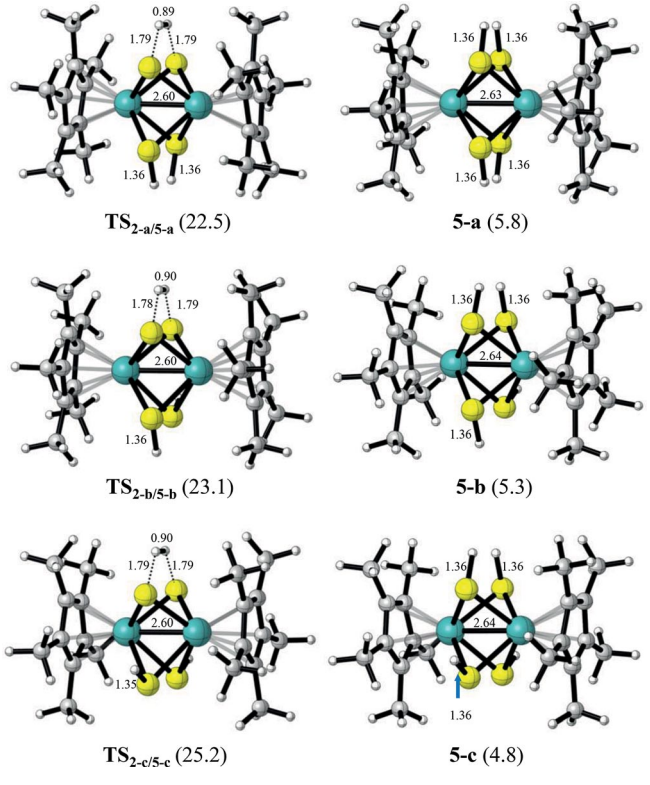

Figure 5. Geometries of the possible isomers of $[Cp_2Mo_2(\mu\text{-}SH)_4]$ (**5-a**, **5-b** and **5-c**) and the transition states for their formation from **2-a**, **2-b** and **2-c**, respectively. The numbers in parentheses correspond to the free energies [kcal mol^{-1}] relative to **2-d** + H_2, and selected distances are given in Å.

Mechanisms involving the direct participation of the molybdenum centres, analogously to Pathways A and B in Scheme 4 for **1-a**, have also been computed starting from **2-d**. The calculations show that H_2 can coordinate to one of the molybdenum centres of **2-d** to form species **7** (+37.3 kcal mol^{-1}); however, to accommodate this ligand, the core of the dinuclear cluster has to open and, consequently, there is an energetic penalty. The structures and free-energy profile associated with the formation of the dihydrogen complex **7** is shown in Figure 6; this process also implies the concerted cleavage of a Mo–S bond and, therefore, the formation of a terminal sulfur ligand at the adjacent molybdenum centre (TS**2-d/7**, +43.6 kcal mol^{-1}). Conversely, despite many attempts to locate a transition state for the addition of H_2 across a Mo–(μ-S) bond of **2-d**, no TS for the direct formation of **8** from **2-d** and H_2 could be located. Instead, it was found that **7** can isomerise into **8** (+29.8 kcal mol^{-1}) via a transition state (TS**7/8**, +41.1 kcal mol^{-1}) that features the transfer one of the H atoms of the dihydrogen ligand to the terminal sulfur atom of the

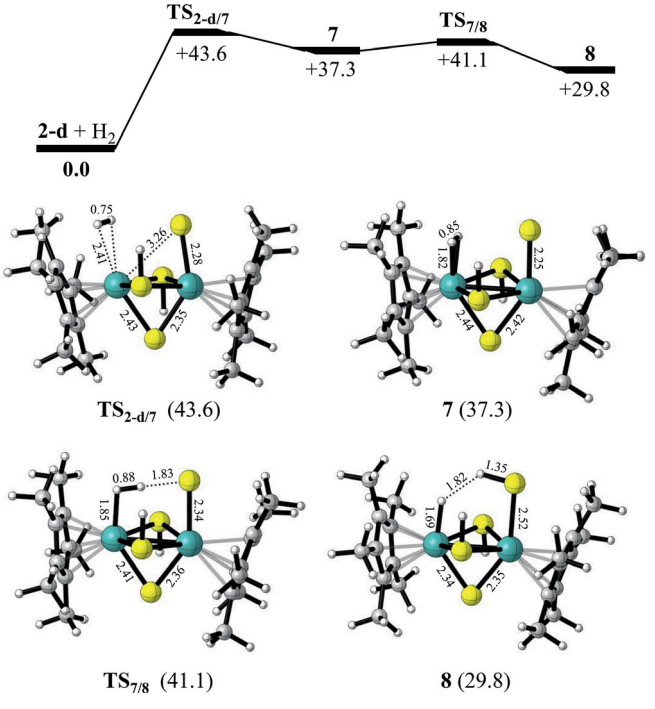

Figure 6. Computed free-energy profile [kcal mol^{-1}] for the reaction of **2-d** with H_2 to generate **7** and **8**. Selected distances are given in Å.

adjacent metal centre. Overall, the relative free energies of **7** and **8**, as well as those of the transition states for their formation, indicate that such species are unlikely to be involved in the H_2/D_2 isotope exchange process.

The computational results indicate that the most plausible mechanism for the generation of HD in the presence of H_2 and D_2 implies the isomerisation of **2-d** into either **2-a**, **2-b** or **2-c**, followed by their reaction with H_2 to form one of the corresponding isomers of $[Cp_2Mo_2(\mu\text{-}SH)_4]$, that is, **5-a**, **5-b** or **5-c**. The interconversion between these represents the last step required to account for the cluster-catalysed formation of HD, and two transition states TS**5-a/5-b** and TS**5-b/5-c** (Figure 7) that only differ in the orientation of one of the hydrosulfido ligands have been found to account for this process. In contrast to the TSs for the analogous step for $[Cp^*Mo]_2(\mu\text{-}S)_2(\mu\text{-}SH)_2$ (i.e., TS**2-a/2-b**, TS**2-b/2-c** and TS**2-d/2-e**), which required the opening of the cluster core, no significant cluster distortions are observed in this case. Both structures show the hydrogen atom to be transferred in the plane formed by the sulfur atom to which it is bound and the molybdenum centres (equatorial plane of the structures in Figure 7). Energetically, TS**5-a/5-b** and TS**5-b/5-c** lead to very similar free-energy barriers (+32.6 and +32.4 kcal mol^{-1}, quoted relative to **2-d** + H_2), and this represents the rate-determining step for the whole HD formation process. Taken together, these results allows to propose the mechanism depicted in Figure 8 for the formation of HD in the presence of $[Cp^*Mo]_2(\mu\text{-}S)_2(\mu\text{-}SH)_2$. Initially, isomerisation of **2-d** leads to **2-c**, which can then react with D_2 to generate **5-c**. The intramolecular rearrangement of **5-c** via TS**5-b/5-c** in the rate-determining step leads to **5-b**, which can then eliminate a HD molecule to form a monodeuterated isomer of **2-b**. This species can further rearrange into the more stable **2-e** and finally **2-d** to close the catalytic cycle.

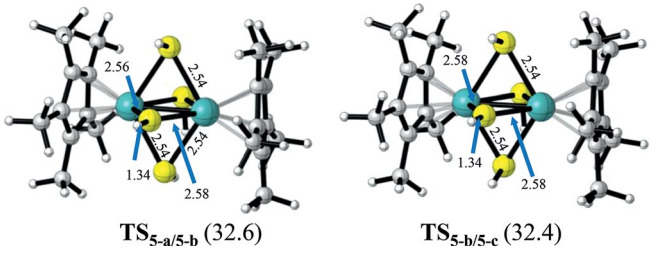

Figure 7. Geometries of the transition states for the interconversion between the isomers of $[Cp_2Mo_2(\mu\text{-}SH)_4]$. The numbers in parentheses correspond to free energies [kcal mol^{-1}] relative to **2-d** + H_2, and selected distances are given in Å.

Conclusions

A thorough computational study on the structure and reactivity of **1-a** and the isomers of **2** with H_2 is presented in this article. The analysis of the possible mechanistic pathways for the reaction between **1-a** and H_2 shows that the molybdenum centres are not directly involved in the product formation. Instead, **2-a** is likely to result from a stepwise mechanism that implies the initial homolytic addition of H_2 to the sulfido ligands of **1-a**, followed by a second step in which the S–S bond of the $\mu\text{-}S_2$ ligand is cleaved. Both steps present similar computed activation free-energy barriers of 17.4 kcal mol^{-1}, and overall the formation of **2-a** is exergonic by 3.1 kcal mol^{-1}. Notably, these results are in sharp contrast with those for the reactivity of the analogous species $CpMo(\mu\text{-}SH)(\mu\text{-}S)(\mu\text{-}S_2CH_2)MoCp$, which adds H_2 across a single Mo–S bond,[10] and it could be hypothesised that the different behaviour is related to the lack of adjacent sulfido ligands in the latter compound.

Complex **2** can exist in five different conformations that only differ in the stereochemistry of the μ-SH and μ-S ligands. Although **2-a** is initially formed during the reaction, it subsequently isomerises into the remaining isomers via transition states with relative free energies that roughly coincide with that for the formation of **2-a**. Of those, **2-d** is computed to be the most stable isomer, and its formation is calculated to be exergonic by 11.3 kcal mol^{-1}. In agreement with experimental data showing that **2-d** does not further add H_2, the computation of

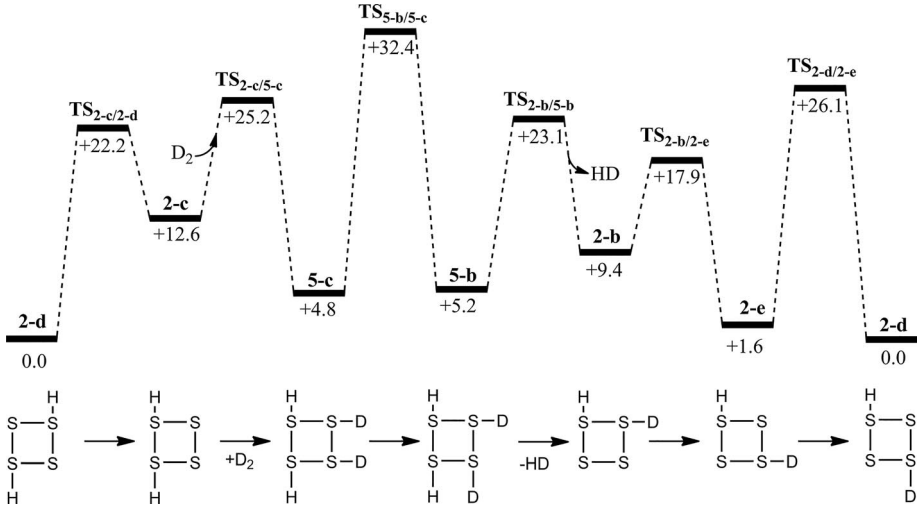

Figure 8. Computed free-energy profile [kcal mol^{-1}] for the most plausible mechanism for the formation of HD in the presence of $[Cp^*Mo]_2(\mu\text{-}S)_2(\mu\text{-}SH)_2$. For clarity, the structures have been represented as the square formed by their four sulfur atoms.

several mechanistic possibilities for such process shows that they all feature prohibitive activation free-energy barriers and positive reaction energies. Nonetheless, the analysis of the reaction of H_2 with the isomers of $[Cp^*Mo]_2(\mu\text{-}S)_2(\mu\text{-}SH)_2$ that feature adjacent sulfido ligands (i.e., **2-a**, **2-b** and **2-c**) shows that these species can activate H_2 homolytically with moderate activation barriers. The isomerisation of the resulting tetra(hydrosulfido)-complexes of formula $[Cp_2Mo_2(\mu\text{-}SH)_4]$, which serve as models for $[Cp_2Mo_2(\mu\text{-}SH)_2(\mu\text{-}SD)_2]$, is the rate-determining step ($\Delta G^{\#}$ = 32.4 kcal mol^{-1}) of a catalytic cycle that explains the experimental observation of HD when a mixture of H_2 and D_2 is bubbled into a solution of $[Cp^*Mo]_2(\mu\text{-}S)_2(\mu\text{-}SH)_2$. The proposed mechanism consists of the initial interconversion of **2-d** into one of its isomers with two adjacent sulfido ligands, the homolytic activation of D_2 by one of these species to form $[Cp_2Mo_2(\mu\text{-}SH)_2(\mu\text{-}SD)_2]$ and the rate-determining interconversion between the isomers of such a tetra(hydrosulfido) complex.

Finally, it is worth noting that H_2 activation and H_2/D_2 isotope exchange processes are also catalysed by the MoS_2 nanoparticles typically employed for hydrotreating, and certain similarities with them have been pointed out. Therefore, the results presented herein could be of use for a better understanding of the processes that occur at such solid phases.

Computational Details

All calculations were performed with Gaussian 09 (rev. D.01)[32] and the B3LYP functional.[33] Geometry optimisations were performed with a basis-set system (BS1) that employs the SDD relativistic effective core potential (ECP), an associated basis set for Mo and S atoms[34] with added polarisation functions for the latter (ζ = 0.503)[35] and the 6-31G** basis set for C, O and H atoms.[36] The ultrafine integration grid option of Gaussian 09 was employed in all geometry optimisations. The effect of the functional on the computed geometry of **1-a**, for which an X-ray structure is available,[19] was tested, and the results can be found in the Supporting Information (Table S1). Frequency calculations were performed at the same level of theory to obtain free-energy corrections at 298.15 K and 1 atm pressure and to confirm the nature of each stationary point. Intrinsic reaction coordinate (IRC) calculations and subsequent geometry optimisations were employed to confirm the minima linked by each transition state. Dispersion corrections as well as those for the effects of the solvent were computed as single-point calculations on the optimised structures. The former employed the Grimme D3BJ parameter set,[37] whereas the latter made use of the polarisable continuum model (PCM) at the B3LYP/BS1 level of theory (chloroform, ε = 4.7113).[38]

To obtain improved energetic values, the gas-phase electronic energies were recomputed through single-point calculations with a larger basis-set system (BS2), which differs from BS1 in the employment of 6-311+G(2d,2p) for C, O and H atoms. The energies in the text refer to Gibbs free energies in solution and are based on the gas-phase-optimised geometries, subsequently corrected for solvent, dispersion and basis-set effects. Details of the different contributions for each species are given in the Supporting Information (Table S2). Structures were generated with CYLview [colour code: Mo (turquoise), S (yellow), C (grey), H (white)].[39]

The activation strain model (ASM),[40] also known as the distortion/interaction model,[41] was employed to decompose the barriers of some of the H_2 activation processes into the strain $\Delta E^{\#}_{strain}$ of the reactants (i.e., the energy required to deform them into their geometries at the transition-state structures) plus the interaction $\Delta E^{\#}_{int}$ between these deformed reactants. Basis-set-corrected (BS2) gas-phase electronic energies were employed for this purpose.

Acknowledgments

Financial support from the European Union (EU) (FEDER program, project number CTQ2012-37821-C02) is acknowledged. The University of Cádiz is acknowledged for the provision of computing resources. Prof. M. G. Basallote is acknowledged for useful comments.

Keywords: Density functional calculations · Reaction mechanisms · Homogeneous catalysis · Dihydrogen · Hydrogen activation · Molybdenum

[1] a) A. Infantes-Molina, A. Romero-Pérez, D. Eliche-Quesada, J. Mérida-Robles, A. Jiménez-López, E. Rodríguez-Castellón, *Transition Metal Sulfide Catalysts for Petroleum Upgrading - Hydrodesulfurization Reactions*, in: *Hydrogenation*, **2012**, DOI: 10.5772/45629; b) R. J. Angelici, *Hydrodesulfurization & Hydrodenitrogenation*, in: *Encyclopedia of Inorganic Chemistry* (Ed. R. B. King), John Wiley & Sons, New York, **2006**; c) E. I. Stiefel, K. Matsumoto (Eds.), *Transition Metal Sulfur Chemistry*, American Chemical Society, Washington DC, **1996**.

[2] a) Y. Zheng, Y. Jiao, M. Jaroniec, S. Z. Qiao, *Angew. Chem. Int. Ed.* **2015**, *54*, 52–65; *Angew. Chem.* **2015**, *127*, 52; b) Y. Huang, R. J. Nielsen, W. A. Goddard, M. P. Soriaga, *J. Am. Chem. Soc.* **2015**, *137*, 6692–6698; c) D. Merki, X. Hu, *Energy Environ. Sci.* **2011**, *4*, 3878–3888; d) L. P. Hansen, Q. M. Ramasse, C. Kisielowski, M. Brorson, E. Johnson, H. Topsøe, S. Helveg, *Angew. Chem. Int. Ed.* **2011**, *50*, 10153–10156; *Angew. Chem.* **2011**, *123*, 10335; e) T. F. Jaramillo, K. P. Jørgensen, J. Bonde, J. H. Nielsen, S. Horch, I. Chorkendorff, *Science* **2007**, *317*, 100–102; f) B. Hinnemann, P. G. Moses, J. Bonde, K. P. Jørgensen, J. H. Nielsen, S. Horch, I. Chorkendorff, J. K. Nørskov, *J. Am. Chem. Soc.* **2005**, *127*, 5308–5309.

[3] a) K. Heinze, *Coord. Chem. Rev.* **2015**, *300*, 121–141; b) G. Schwarz, R. R. Mendel, M. W. Ribbe, *Nature* **2009**, *460*, 839–847; c) R. Hille, *Essays Biochem.* **1999**, *34*, 125–137.

[4] a) W. Lubitz, H. Ogata, O. Rudiger, E. Reijerse, *Chem. Rev.* **2014**, *114*, 4081–4148; b) T. Xu, D. Chen, X. Hu, *Coord. Chem. Rev.* **2015**, *303*, 32–41.

[5] a) Z. Huang, W. Luo, L. Ma, M. Yu, X. Ren, M. He, S. Polen, K. Click, B. Garrett, J. Lu, K. Amine, C. Hadad, W. Chen, A. Asthagiri, Y. Wu, *Angew. Chem. Int. Ed.* **2015**, *54*, 15181–15185; *Angew. Chem.* **2015**, *127*, 15396; b) D. Recatalá, R. Llusar, A. L. Gushchin, E. A. Kozlova, Y. A. Laricheva, P. A. Abramov, M. N. Sokolov, R. Gómez, T. Lana-Villarreal, *ChemSusChem* **2015**, *8*, 148–157; c) J. Kibsgaard, T. F. Jaramillo, F. Besenbacher, *Nat. Chem.* **2014**, *6*, 248–253; d) H. I. Karunadasa, E. Montalvo, Y. Sun, M. Majda, J. R. Long, C. J. Chang, *Science* **2012**, *335*, 698–702; e) M. V. Jiménez, F. J. Lahoz, L. Lukešová, J. R. Miranda, F. J. Modrego, D. H. Nguyen, L. A. Oro, J. J. Pérez-Torrente, *Chem. Eur. J.* **2011**, *17*, 8115–8128; f) T. F. Jaramillo, J. Bonde, J. Zhang, B.-L. Ooi, K. Andersson, J. Ulstrup, I. Chorkendorff, *J. Phys. Chem. C* **2008**, *112*, 17492–17498; g) T. B. Rauchfuss, *Inorg. Chem.* **2004**, *42*, 14–26.

[6] R. C. Linck, R. J. Pafford, T. B. Rauchfuss, *J. Am. Chem. Soc.* **2001**, *123*, 8856–8857.

[7] R. Waterman, *Organometallics* **2013**, *32*, 7249–7263.

[8] a) Z. K. Sweeney, J. L. Polse, R. G. Bergman, R. A. Andersen, *Organometallics* **1999**, *18*, 5502–5510; b) Y. Ohki, M. Sakamoto, K. Tatsumi, *J. Am. Chem. Soc.* **2008**, *130*, 11610–11611; c) A. Ienco, M. J. Calhorda, J. Reinhold, F. Reineri, C. Bianchini, M. Peruzzini, F. Vizza, C. Mealli, *J. Am. Chem. Soc.* **2004**, *126*, 11954–11965.

[9] L. L. Lopez, P. Bernatis, J. Birnbaum, R. C. Haltiwanger, M. Rakowski DuBois, *Organometallics* **1992**, *11*, 2424–2435.

[10] J. E. McGrady, J. Gracia, *J. Organomet. Chem.* **2005**, *690*, 5206–5214.

[11] a) F. Olechnowicz, G. L. Hillhouse, R. F. Jordan, *Inorg. Chem.* **2015**, *54*, 2705–2712; b) J. Á. Pino-Chamorro, A. L. Gushchin, M. J. Fernández-Tru-

jillo, R. Hernández-Molina, C. Vicent, A. G. Algarra, M. G. Basallote, *Chem. Eur. J.* **2015**, *21*, 2835–2844; c) E. Bustelo, A. L. Gushchin, M. J. Fernández-Trujillo, M. G. Basallote, A. G. Algarra, *Chem. Eur. J.* **2015**, *21*, 14823–14833; d) J. P. Collman, L. M. Slaughter, T. A. Eberspacher, T. Strassner, J. I. Brauman, *Inorg. Chem.* **2001**, *40*, 6272–6280.

[12] M. Rakowski DuBois, *Chem. Rev.* **1989**, *89*, 1–9.

[13] a) M. Rakowski DuBois, B. Jagirdar, B. Noll, S. Dietz, *Syntheses, Structures, and Reactions of Cyclopentadienyl Metal Complexes with Bridging Sulfur Ligands*, in: *Transition Metal Sulfur Chemistry*, American Chemical Society, Washington DC, **1996**, p. 269–281; b) P. Bernatis, R. C. Haltiwanger, M. Rakowski DuBois, *Organometallics* **1992**, *11*, 2435–2443; c) L. L. Wright, R. C. Haltiwanger, J. Noordik, M. Rakowski DuBois, *J. Am. Chem. Soc.* **1987**, *109*, 282–283; d) R. T. Weberg, R. C. Haltiwanger, J. C. V. Laurie, M. Rakowski DuBois, *J. Am. Chem. Soc.* **1986**, *108*, 6242–6250; e) J. C. V. Laurie, L. Duncan, R. C. Haltiwanger, R. T. Weberg, M. Rakowski DuBois, *J. Am. Chem. Soc.* **1986**, *108*, 6234–6241; f) W. K. Miller, R. C. Haltiwanger, M. C. VanDerveer, M. Rakowski DuBois, *Inorg. Chem.* **1983**, *22*, 2973–2979; g) M. McKenna, L. L. Wright, D. J. Miller, L. Tanner, R. C. Haltiwanger, M. Rakowski DuBois, *J. Am. Chem. Soc.* **1983**, *105*, 5329–5337; h) M. Rakowski DuBois, R. C. Haltiwanger, D. J. Miller, G. Glatzmaier, *J. Am. Chem. Soc.* **1979**, *101*, 5245–5252; i) R. Newell, C. Ohman, M. Rakowski DuBois, *Organometallics* **2005**, *24*, 4406–4415; j) M. Rakowski DuBois, D. L. DuBois, M. C. VanDerveer, R. C. Haltiwanger, *Inorg. Chem.* **1981**, *20*, 3064–3071; k) M. Rakowski DuBois, M. C. VanDerveer, D. L. DuBois, R. C. Haltiwanger, W. K. Miller, *J. Am. Chem. Soc.* **1980**, *102*, 7456–7461.

[14] C. J. Casewit, D. E. Coons, L. L. Wright, W. K. Miller, M. Rakowski DuBois, *Organometallics* **1986**, *5*, 951–955.

[15] D. L. DuBois, W. K. Miller, M. Rakowski DuBois, *J. Am. Chem. Soc.* **1981**, *103*, 3429–3436.

[16] A. M. Appel, S.-J. Lee, J. A. Franz, D. L. DuBois, M. Rakowski DuBois, B. Twamley, *Organometallics* **2009**, *28*, 749–754.

[17] A. E. Bruce, D. R. Tyler, *Inorg. Chem.* **1984**, *23*, 3433–3434.

[18] a) M. R. M. Bruce, A. E. Bruce, D. R. Tyler, *Polyhedron* **1985**, *4*, 2073–2081; b) B. E. Bursten, R. H. Cayton, *Inorg. Chem.* **1989**, *28*, 2846–2853; c) W. Tremel, R. Hoffmann, E. D. Jemmis, *Inorg. Chem.* **1989**, *28*, 1213–1224.

[19] H. Brunner, W. Meier, J. Wachter, E. Guggolz, T. Zahn, M. L. Ziegler, *Organometallics* **1982**, *1*, 1107–1113.

[20] G. J. Kubas, R. R. Ryan, K. A. Kubat-Martin, *J. Am. Chem. Soc.* **1989**, *111*, 7823–7832.

[21] H. Brunner, H. Kauermann, W. Meier, J. Wachter, *J. Organomet. Chem.* **1984**, *263*, 183–192.

[22] J. A. Franz, J. C. Birnbaum, D. S. Kolwaite, J. C. Linehan, D. M. Camaioni, M. Dupuis, *J. Am. Chem. Soc.* **2004**, *126*, 6680–6691.

[23] The X-ray structure of $Cp^*_2Mo_2S_4H_2$ was fully described in **2009** and assigned to the **2-d** isomer, see ref.[16]

[24] a) A. M. Appel, S.-J. Lee, J. A. Franz, D. L. DuBois, M. Rakowski DuBois, *J. Am. Chem. Soc.* **2009**, *131*, 5224–5232; b) A. M. Appel, S.-J. Lee, J. A. Franz, D. L. DuBois, M. Rakowski DuBois, J. C. Birnbaum, B. Twamley, *J. Am. Chem. Soc.* **2008**, *130*, 8940–8951; c) A. M. Appel, D. L. DuBois, M. Rakowski DuBois, *J. Am. Chem. Soc.* **2005**, *127*, 12717–12726.

[25] W. Danzer, W. P. Fehlhammer, A. T. Liu, G. Thiel, W. Beck, *Chem. Ber.* **1982**, *115*, 682.

[26] This type of structural representation has already been used by Appel et al., see ref.[24b]

[27] W. Koch, in: *A Chemist's Guide to Density Functional Theory*, Wiley, New York, **2000**.

[28] Positive interaction energy values must be considered in the context of the mathematical treatment of strain/interaction energies, that is, the point at which $\delta(\Delta E^{\#}_{strain}) = -\delta(\Delta E^{\#}_{int})$, which can lead to positive $\Delta E^{\#}_{int}$ values; see: D. H. Ess, *J. Org. Chem.* **2009**, *74*, 1498–1508, and references cited therein.

[29] Note that the $Mo_2(\mu\text{-}S_2)$ and $Mo_2(\mu\text{-}S)_2$ moieties of **1-a** are analogous to the 100 % sulfur-covered (10–10) Mo edges and (–1010) S edges of MoS_2.

[30] a) P.-Y. Prodhomme, P. Raybaud, H. Toulhoat, *J. Catal.* **2011**, *280*, 178–195; b) J.-F. Paul, S. Cristol, E. Payen, *Catal. Today* **2008**, *130*, 139–148; c) M. Sun, A. E. Nelson, J. Adjaye, *Catal. Today* **2005**, *105*, 36–43; d) J.-F. Paul, E. Payen, *J. Phys. Chem. B* **2003**, *107*, 4057–4064; e) L. S. Byskov, M. Bollinger, J. K. Nørskov, B. S. Clausen, H. Topsøe, *J. Mol. Catal. A* **2000**, *163*, 117–122; f) Y. Huang, H. Liu, C. Ling, X. Chen, D. Zhou, S. Wang, *J. Phys. Chem. C* **2015**, *119*, 17092–17101.

[31] a) S. Cristol, J. F. Paul, E. Payen, D. Bougeard, S. Clémendot, F. Hutschka, *J. Phys. Chem. B* **2002**, *106*, 5659–5667; b) A. Travert, H. Nakamura, R. A. van Santen, S. Cristol, J.-F. Paul, E. Payen, *J. Am. Chem. Soc.* **2002**, *124*, 7084–7095.

[32] M. J. Frisch, G. W. Trucks, H. B. Schlegel, G. E. Scuseria, M. A. Robb, J. R. Cheeseman, G. Scalmani, V. Barone, B. Mennucci, G. A. Petersson, H. Nakatsuji, M. Caricato, X. Li, H. P. Hratchian, A. F. Izmaylov, J. Bloino, G. Zheng, J. L. Sonnenberg, M. Hada, M. Ehara, K. Toyota, R. Fukuda, J. Hasegawa, M. Ishida, T. Nakajima, Y. Honda, O. Kitao, H. Nakai, T. Vreven, J. A. Montgomery Jr., J. E. Peralta, F. Ogliaro, M. Bearpark, J. J. Heyd, E. Brothers, K. N. Kudin, V. N. Staroverov, R. Kobayashi, J. Normand, K. Raghavachari, A. Rendell, J. C. Burant, S. S. Iyengar, J. Tomasi, M. Cossi, N. Rega, J. M. Millam, M. Klene, J. E. Knox, J. B. Cross, V. Bakken, C. Adamo, J. Jaramillo, R. Gomperts, R. E. Stratmann, O. Yazyev, A. J. Austin, R. Cammi, C. Pomelli, J. W. Ochterski, R. L. Martin, K. Morokuma, V. G. Zakrzewski, G. A. Voth, P. Salvador, J. J. Dannenberg, S. Dapprich, A. D. Daniels, Ö. Farkas, J. B. Foresman, J. V. Ortiz, J. Cioslowski, D. J. Fox, *Gaussian 09*, revision D.01, Gaussian, Inc., Wallingford CT, **2013**.

[33] a) A. D. Becke, *J. Chem. Phys.* **1993**, *98*, 5648–5652; b) C. T. Lee, W. T. Yang, R. G. Parr, *Phys. Rev. B* **1988**, *37*, 785–789.

[34] D. Andrae, U. Haussermann, M. Dolg, H. Stoll, H. Preuss, *Theor. Chim. Acta* **1990**, *77*, 123–141.

[35] A. Hollwarth, M. Bohme, S. Dapprich, A. W. Ehlers, A. Gobbi, V. Jonas, K. F. Kohler, R. Stegmann, A. Veldkamp, G. Frenking, *Chem. Phys. Lett.* **1993**, *208*, 237–240.

[36] a) P. C. Harihanan, J. A. Pople, *Theor. Chim. Acta* **1973**, *28*, 213–222; b) W. J. Hehre, R. Ditchfield, J. A. Pople, *J. Chem. Phys.* **1972**, *56*, 2257–2261.

[37] a) S. Grimme, J. Antony, S. Ehrlich, H. Krieg, *J. Chem. Phys.* **2010**, *132*, 154104; b) S. Grimme, S. Ehrlich, L. Goerigk, *J. Comput. Chem.* **2011**, *32*, 1456–1465.

[38] a) M. Cossi, G. Scalmani, N. Rega, V. Barone, *J. Chem. Phys.* **2002**, *117*, 43–54; b) J. Tomasi, B. Mennucci, R. Cammi, *Chem. Rev.* **2005**, *105*, 2999–3093.

[39] C. Y. Legault, *CYLview*, v. 1.0b, Université de Sherbrooke, Canada, **2009**, http://www.cylview.org.

[40] a) L. P. Wolters, F. M. Bickelhaupt, *Wiley Interdiscip. Rev.: Comput. Mol. Sci.* **2015**, *5*, 324–343; b) I. Fernández, F. M. Bickelhaupt, *Chem. Soc. Rev.* **2014**, *43*, 4953–4967; c) F. M. Bickelhaupt, *J. Comput. Chem.* **1999**, *20*, 114–128; d) F. M. Bickelhaupt, E. J. Baerends, N. M. M. Nibbering, T. Ziegler, *J. Am. Chem. Soc.* **1993**, *115*, 9160–9173.

[41] a) D. H. Ess, K. N. Houk, *J. Am. Chem. Soc.* **2007**, *129*, 10646–10647; b) D. H. Ess, K. N. Houk, *J. Am. Chem. Soc.* **2008**, *130*, 10187–10198.

Received: February 8, 2016
Published Online: March 21, 2016

